Lawrence Berkeley National Laboratory
Chemical Sciences

Title

Nanocrystals of Uranium Oxide: Controlled Synthesis and Enhanced Electrochemical Performance of Hydrogen Evolution by Ce Doping

Authors

Hu, Shi
Li, Haoyi
Liu, Huiling
et al.

Peer reviewed

Nanocrystals of Uranium Oxide: Controlled Synthesis and Enhanced Electrochemical Performance of Hydrogen Evolution by Ce Doping

Shi Hu, Haoyi Li, Huiling Liu, Peilei He, and Xun Wang*

With the progress of synthetic techniques in colloidal nanostructures, especially the ultrathin nanostructures during the past three decades,[1] nanoscientists have been able to adeptly engineer the shape, structure and properties of various materials for applications in the academia and all walks of life.[2] Relentless efforts were devoted to the well-known compounds of main-group elements while actinide elements have been rarely mentioned except for sporadic reports.[3] Actually, actinide compounds were intentionally or unintentionally avoided by material scientists, which could be caused by undeserving fear about their radioactivity and ignorance about their value from the aspect of material science. Among the actinides of which most are synthetic elements, uranium is a promising element to be exploited due to the ultralong radioactive half-life of its isotopes and abundant availability from the nuclear industry. Large amount of depleted uranium has been produced every year while inappropriate treatment of the waste has raised certain problems concerning its potential hazard to the environment. Apart from the traditional use as fuel in nuclear plants, uranium compounds were recently shown to possess great potential in solar-cell applications and integrated-circuits material[4] over the conventional materials such as Si and GaAs, thanks to the appropriate bandgaps of these uranium oxides. In addition, UO_2 is also one of the most favorable thermoelectric materials with a combined feature of high Seebeck coefficient and good thermal and electric conductivity. It also displays high efficiency in many catalytic reactions due to its hybridized 5f-orbital electrons.[5]

Up to now, the study of nanostructured uranium compounds has been quite limited, especially for ultrathin structures when quantum confinement could significantly change the electric, optical, and chemical properties.[6] Previous research in this area typically focused on the generation, transport, and environmental impact of the nanoparticles of uranium compounds[7] while serious reports on uranium-based nanostructures from the aspect of material science were not seen before the size-controllable synthesis of monodisperse nanoparticles of UO_2 and UO_2–In_2O_3

heterostructure in coordinating solvent were presented by Cao and co-workers.[3a,b] Their reports on the growth of isotropic UO_2 nanoparticles have intrigued little response due to limited control over the structure and morphology.[8] In this article, we demonstrate a successful control over the morphology and structure of uranium oxides, including zero-dimensional (0D) nanoparticles of UO_2, one-dimensional (1D) ultrathin nanowires of U_3O_7, and two-dimensional (2D) ultrathin nanoribbons of U_3O_8 with combined low-temperature hydrothermal method and flask-reaction. In addition, cerium doping was found to have direct effects on the morphology and enhanced electrochemical performance in hydrogen evolution as compared to the above-mentioned nanostructures. This work is going to enrich the library of ultrathin semiconductor nanomaterials and promote the wide study of uranium compounds and utilization of spent uranium waste.

As the most stable form of uranium oxide, spherical-shaped nanoparticles of UO_2 were successfully obtained in previous work.[3a] However, isotropic growth of nanoparticles significantly limits the use and applications of the material and symmetry breaking can provide more possibilities. In order to obtain 2D ultrathin nanoribbons, uranium acetate was dissolved in a mixture of oleylamine (OM) and oleic acid (OA) and heated in a flask within oil bath; the product was collected by centrifuging after cooling. After washing with ethanol, the final product was dispersed in cyclohexane and characterized by transmission electron microscopy (TEM). High-purity ultrathin nanoribbons were obtained after 4-h reaction, as shown in **Figure 1**a. The nanoribbons were featured with uniform width of 4 nm and length from 100 to 200 nm. By adding ethanol to the cyclohexane dispersion, the nanoribbons were precipitated on the grid showing uniform thickness of 1 nm (Figure 1b), due to enhanced surfactant interaction between facing sides of ribbons. The lattice fringes in the high-resolution transmission electron microscopy (HRTEM) images (Figure 1c) correspond to the (111) interplanar spacing of fluorite UO_2 while the X-ray diffraction (XRD) pattern of the solid sample was clearly indexed to U_3O_8 (JCPDS No. 08-0244) which features a layered structure (Figure 1g). This kind of discrepancy can be attributed to the electron-beam-induced rapid reduction of U_3O_8 into UO_2. While beam-induced structure change in oxide nanostructures has also been found in the TEM results of some other materials,[9] the reduction process becomes faster in the case of ultrathin nanostructures.

Dr. S. Hu, H. Li, H. Liu, P. He, Prof. X. Wang
Department of Chemistry
Tsinghua University
Beijing 100084, China
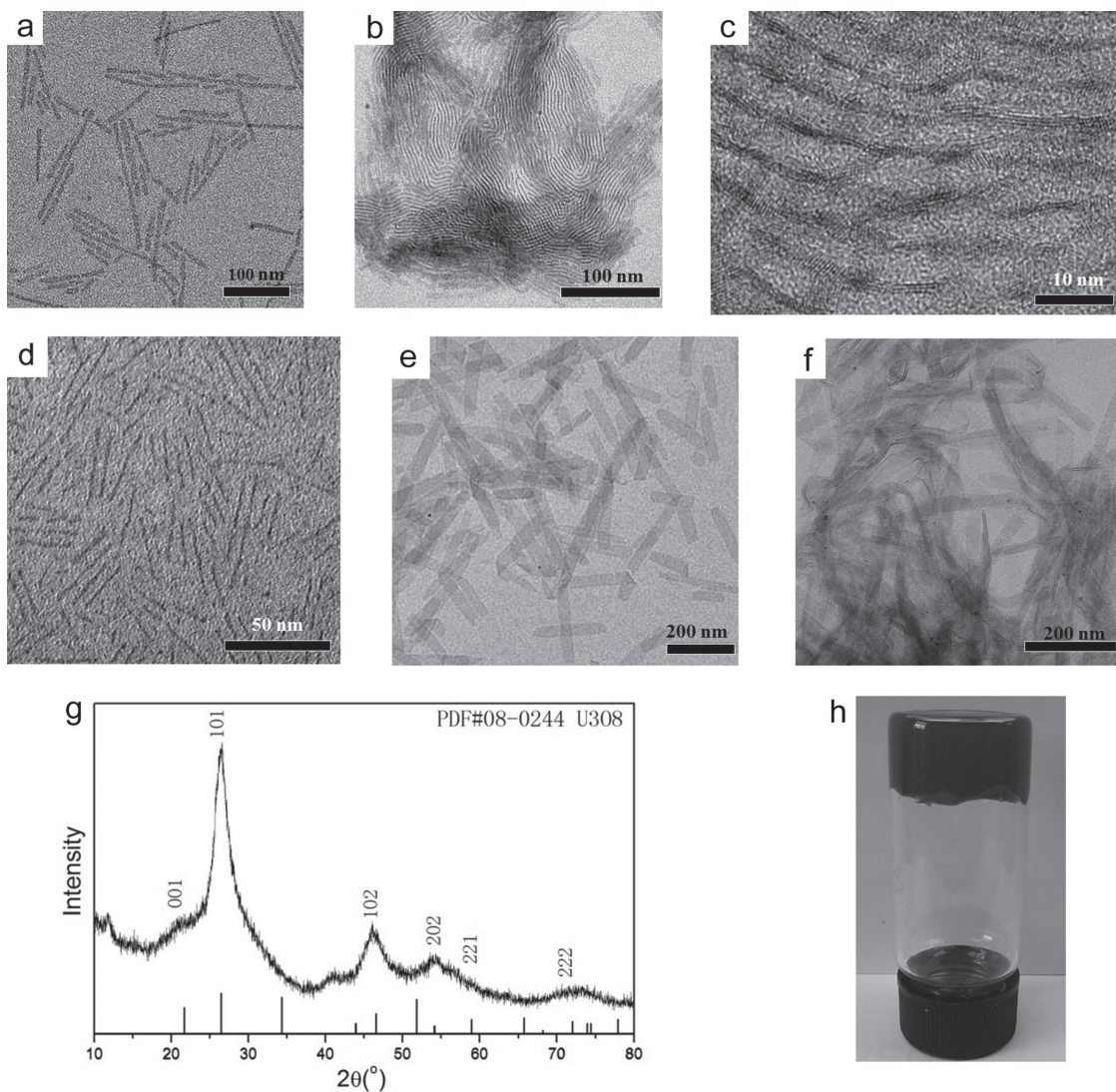E-mail: wangxun@mail.tsinghua.edu.cn

Figure 1. a) TEM images of as-prepared ultrathin nanoribbons (thickness less than 1 nm, width around 4 nm). b) TEM and c) HRTEM images of the same sample in assembly state. TEM images of ultrathin nanoribbons with d) smaller width prepared in flask with condenser and e) larger width prepared in autoclaves. f) TEM image of side-viewed nanoribbons assembly. g) XRD pattern of the sample in a) with the peak position of U3O8 marked at the bottom. h) Organogel formed from highly concentrated cyclohexane dispersion of nanoribbon sample in e).

It should be noted that the thickness of the nanoribbons is fairly constant with a lower or higher reaction temperature and it could be related to the templating effect of OA and OM in the reaction system. However, the width of nanoribbon can be controlled by tuning the pressure of reaction system. When the same reactant mixture is sealed in an autoclave with autogenous pressure, the products are wide nanoribbons ($\approx$40 nm) with the same 1-nm thickness, as shown in Figure 1e,f. On the contrary, releasing the partial pressure by replacing the cap with a condenser over the flask could decrease the width of the nanoribbons down to 2 nm and the length to less than 100 nm due to decreased pressure (Figure 1d). Pressure-induced morphology tuning is rarely seen and studied, while in our case it might be related to the pressure-dependent structure of the OA–OM soft-template in the reaction media. The XRD patterns of these nanoribbons with different width are identical and well-indexed to U_3O_8, as illustrated in Figure 1g. The high-aspect-ratio

flexible nanoribbons show strong inter-ribbon interaction in organic solvent (such as cyclohexane) through van der Waals force and could form organogel in high concentration through the formation of 3D entangled network, similar to a recent report of our group on ultrathin nanowires of rare earth hydroxide.[1h] A picture of the as-formed gel is shown in Figure 1h.

On the basis of our research, longer reaction time or enhanced reaction temperature will cause the further reduction of U_3O_8 and hence destroy the layered structures; various oxides with modified UO_2 structure (fluorite) will be generated. However, it is not favorable for fluorite structure to form 1D nanowires, according to a previous survey.[6b] In our method, a third solvent was introduced into the previous autoclave reaction system of pure OA and OM and the temperature was increased to enhance the reduction of uranium. As shown in **Figure 2** and Figure S1, Supporting Information, high-purity (over 95%) ultrathin nanowires were obtained by
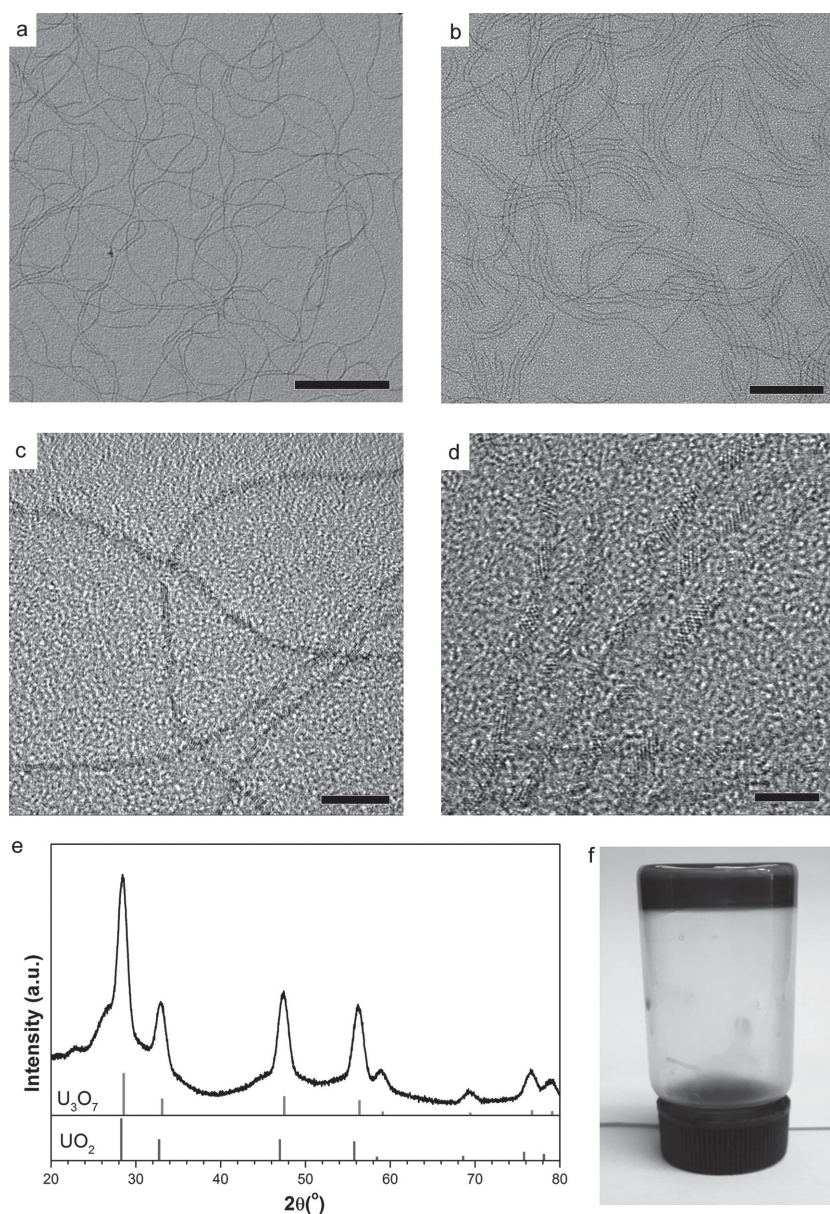
Figure 2. TEM images of 1-nm nanowires of U_3O_7 with controllable length from a) over 500 nm to b) around 50 nm, with corresponding HRTEM images shown in c,d). The scale bars in a–d) are 100, 50, 10, and 5 nm, respectively. e) XRD pattern of a) is indexed to U_3O_7 with UO_2 in comparison. h) Organogel formed from highly concentrated cyclohexane dispersion of nanowires.

introducing octadecene (ODE) as cosolvent. The diameter of these nanowires is constantly around 1 nm and its length could be tuned from around 50 to over 500 nm by changing reaction temperature and time, as shown in Figure 2a,b. It is found that similar reaction in toluene tends to produce short nanowires as compared to the long ones in ODE (Figure S2, Supporting Information). Nevertheless, the structures are identical and the width of these wires is constant at 1 nm. Due to the extreme small width of the nanowires, they could be easily damaged under high electron dosage, as shown in the broken part of the nanowires in Figure 2c,d, from which visible lattice fringes of UO_2 (111) planes could be identified. Small fractions of nanoparticles may coexist in

the product and are difficult to be eliminated completely. The diffraction peaks are well indexed to U_3O_7 (JCPDS No. 75-0456), which is a hyperstoichiometric derivative structure of UO_2 (JCPDS No. 41-1422).[10] These nanowires are highly intertwined in high-concentration dispersion and could form organogel after aging for a few days (Figure 2f), which is similar to the ultrathin nanoribbons.

For the synthesis of high-purity ultrathin nanowires, reaction temperature, reaction time especially the solvent composition have great essential influence on the nanowires–nanoparticles ratio and the length of the nanowires. Actually, a few common solvents have been tested for their selectivity in the growth of ultrathin nanowires. Similar to ODE, other nonpolar solvents such as toluene, cyclohexane, *n*-hexane, *n*-heptane, *n*-decane, etc., all yield nanoparticle–nanowire mixture, with the only difference in the nanoparticle/nanowire ratio and length of the nanowires, as was shown in Figure S2, Supporting Information. On the contrary, replacing octadecene with strongly polar solvent, such as acetone or acetonitrile would only produce nanoparticles, as shown in Figure S3a,b, Supporting Information. In chloroform which is a moderately polar solvent, nanoparticles tend to grow bigger and agglomerate while coexisting nanowires typically grow to hundreds of nanometers long and hence appeared extremely flexible in TEM images, as shown in Figure S3c,d, Supporting Information. We hypothesize that the increase of solvent polarity and weakening of template stability would facilitate the diffusion of U species to the existing NW and hence yield longer NW. The ratio of nanowires will slightly decrease if the reaction temperature is increased, as shown in Figure S4a, Supporting Information.

In addition, the nanowires are constantly 1 nm thin although the ratio and length of nanowires vary with different solvents, different reaction temperature and time. The uniform width could be related to the assembly structure of ligands in solvents, which confines the growth of the uranium monomer into nanowires and nanoparticles of uranium oxide, as shown in Figure S5, Supporting Information. In the proposed assembly template, ligands (OA and OM) tend to bind to uranium species in the core with their polar head groups while exposed to the solvent with the nonpolar alkane chain. Uranium monomers UO_2L_2 (L = OA/OM) can only attach to the uncapped positions on the growing nanowires and nanoparticles. The stability of the template was determined by the
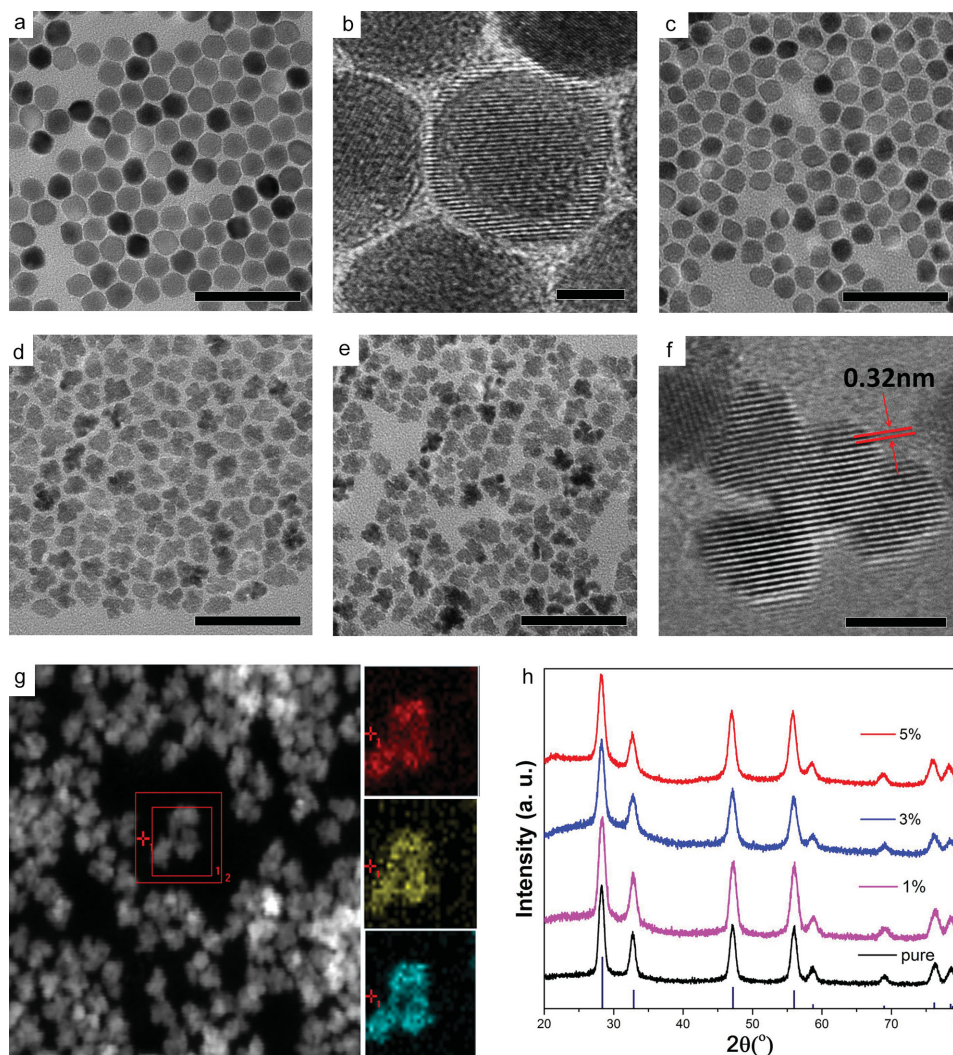
Figure 3. a,c–e) TEM images of pure uranium oxide nanoparticles and nanoparticles with Ce doping (1%, 3%, 5%); the scale bars are 50 nm. b,f) are the HRTEM images of nanoparticles in a,d); the scale bars are 5 nm. g) STEM image and elemental mapping of O, Ce and U (from top down) in the multipod nanoparticles in d). h) Comparison of XRD patterns of pure nanoparticle and Ce-doped (1%, 3%, and 5%) nanoparticles; the diffraction lines are from UO₂ (JCPDS No. 41-1422).

ligand–solvent interaction and hence polarity of the organic media: highly polar media could destabilize the 1D assembly structure, expose more surfaces of the nuclei, and promote further growth of nuclei in all directions while weakly polar solvents stabilize the assembly and overgrowth is slow and 1D. For nonpolar solvents, the OA/OM ligands form stable interdigitated coating on the nanowires and only those at both ends could detach and give rise to further 1D growth. With increasing amount of OA, the 1D template becomes less stable and the growth of nanoparticles is favored. This transition is demonstrated in both ODE and cyclohexane system, as shown in Figure S4b,d, Supporting Information.

Doping of semiconductor nanostructure could alter the energy-band structure and hence induce quite meaningful changes in their properties. Considering the same fluorite structure of CeO_2 and UO_2, it appears viable to obtain Ce-doped uranium oxide nanostructure under similar conditions. Actually, Ce-doping significantly changes the morphology of uranium oxide nanoparticles while the morphology of nanowires

and nanoribbons remains the same after Ce-doping. It is reasonable as the nanowires and nanoribbons are believed to grow in soft template and hence the morphology is predetermined while NPs are only weakly confined by the OA–OM molecule shell and have a lot of exposed surface for coalescence. Monodisperse nanoparticles of uranium oxide were synthesized first and systematic doping of Ce was conducted under identical reaction conditions. As shown in **Figure 3**a,b, undoped nanoparticles show a uniform size around 9 nm and the lattice fringes in the HRTEM correspond to the spacing between (111) planes of UO_2, i.e., 0.32 nm. As for Ce-doping, 1%–2% does not bring about obvious change to the near-spherical morphology of the polyhedral nanoparticles; however, the nanoparticles shape tends to be more irregular, as shown in Figure 3c. When the doping level reaches 3%, polyhedral nanoparticles changed to multipod shape (Figure 3d) while further increase in doping percentage (5% and up to 10%) does not make obvious differences (Figure 3e and Figure S6, Supporting Information). HRTEM images in Figure 3f clearly show the

lattice orientation across the multipod nanoparticles, indicating a possible mechanism of oriented attachment. The highlighted multipod nanoparticles seem to be formed by the merging of four primary nanoparticles with well-aligned crystal direction over opposing (111) planes which are densely packed atomic planes with an interplanar spacing of 0.32 nm. The XRD patterns of all the doped samples (up to 5%) in Figure 3h could be indexed to UO_2 (JCPDS No. 41-1422) as well as CeO_2 without noticeable peak shift with that of the undoped one. It would be hard to differentiate between them considering the low doping level and comparable ionic radius of Ce^{4+} (101 pm) and U^{4+} (103 pm).[11] The tremendous morphology evolution brought about by Ce-doping could be caused by the varied stability and ligand coverage of the Ce-doped primary nanoparticles; the steady growth toward polyhedron is interrupted and oriented attachment happens, typically along the <111> directions. Actually, doping-induced morphology change is not uncommon and it is generally believed that dopants are involved in the nucleation and growth through modified process of aggregation and diffusion.[12] The control experiment from equal amount of Ce precursor (without any uranium) does not yield any precipitate under identical reaction conditions, which indicates a more stable Ce–ligand bonding as compared to U–ligand with reference to their oxides. It would be reasonable to believe that a preferential bonding of OA/OM with surface Ce-sites dominates the doped CeO_2 nanocrystals and this is what we believe could influence the surface distribution of ligands on primary nanocrystals and the stability of exposed surface and aggregation mode of doped uranium oxide.

To obtain a clearer understanding of the growth of the multipod nanoparticles, we further compared the morphology of products with different temperature and reaction time by controlling the doping level at 5% through TEM imaging. As shown in Figure S7a,b, Supporting Information, more branches were found in the 8-h products as compared to the 4-h ones but 12-h products become more rounded than the 8-h ones (Figure S7c, Supporting Information). Furthermore, nanoparticles obtained at higher temperature (Figure S7d, Supporting Information, for 170 °C and Figure S6e, Supporting Information, for 180 °C) become even smoother. This morphology evolution might be caused by the atomic migration which happens at the same time with the

oriented attachment and the multipod nanoparticle has a tendency to become more rounded by rubbing out the protruding pods with prolonged reaction time, as shown in Figure S7c, Supporting Information, and this coarsening process gets even faster at higher temperature, as shown in Figure S7d,e, Supporting Information. Reaction at even higher temperature of 200 °C could ruin the oriented attachment growth and large disordered aggregate of tiny nanoparticles shows up in Figure S7f, Supporting Information.

The semiconducting uranium oxide nanostructures provide the test field for quite a lot of applications which have rarely been explored. As a preliminary demonstration, the electrocatalytic performance of the above materials in hydrogen evolution reaction (HER) was evaluated. These samples were deposited on glassy carbon electrodes and tested in a typical three-electrode electrochemical system (see Experimental Section). As shown in the polarization curve (*I–V* plot) of **Figure 4**a, the onset overpotentials of 3% Ce-doped multipod nanoparticles were around 370 mV versus reversible hydrogen electrode (RHE) with 1% ones slightly more negative and 5%–10% even worse, as compared to about −500 mV for pure nanoparticles; nanoribbons, and nanowires have almost no response. The phenomenon shows that the intrinsic HER electrocatalytic activity of uranium oxides is relatively low while Ce-doping will significantly improve that, especially obvious from 1% to 3%. However, the enhancement effect of doping is not unlimited and peaks around the level of 3% as the performance declines from 3% through 5% to 10%. On the other hand, the alternating current impedance spectroscopy of all these samples were tested and shown in Figure 4b. The best-performing multipod nanoparticles with 3% Ce-doping shows the lowest impedance value while the impedance of 5% and 10% doped nanoparticles was significantly higher, which also applies to pristine nanoparticles, nanowires, and nanoribbons. As compared to pristine nanoparticles, branched nanoparticles (3% Ce-doping) have relatively larger surface area which is supposed to contribute to the overall high performance. To the contrary, the surface of ultrathin nanowires and nanoribbons are well-protected by the organic ligands in solvents and the HER performance is even poorer than nanoparticles. However, surface area is definitely not the sole factor as
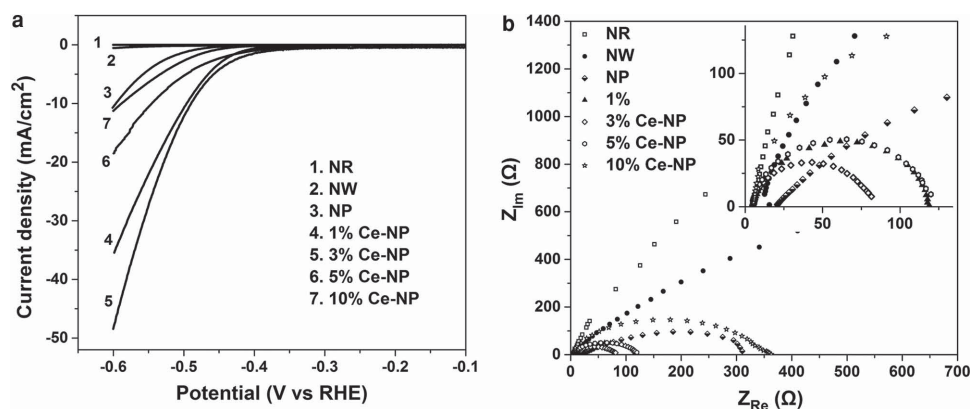

Figure 4. a) The polarization curves and b) alternating current impedance spectra of different nanostructures of uranium oxides including nanoribbons (NR), nanowires (NW), pristine nanoparticle (NP), and Ce-doped nanoparticles (Ce-NP). The inset is a zoom-in of b).

1% Ce-doped sample also shows significantly enhanced performance without remarkable change in the morphology. Actually, varied surface sites and energy band structure caused by doping might play a complicated or even contradictive role as witnessed by the performance decline with further increasing doping levels, considering the same branch structure and similar surface area for 3%, 5%, and 10% doped nanoparticles. The increased surface area definitely contributes to the overall performance but it is not feasible for us to evaluate this contribution separately from other factors as it requires fine-tuning of surface area for every kind of nanostructure, including nanowires, nanoribbons, and doped/pristine nanoparticles. Although these preliminary results for HER electrochemical performance of the uranium oxide are far from inspiring, further improvement can be expected.

In summary, multiple growth methods were utilized for the synthesis of the high-quality 0D, 1D, and 2D nanostructures of uranium oxide. Ultrathin nanoribbons of U_3O_8 with controllable width were fabricated in an OA–OM coordinating solvent by tuning the pressure of the reaction system at a lower temperature. The introduction of proper solvent and higher temperature in autoclaves induced the anisotropic growth of ultrathin nanowires of U_3O_7 with high purity and controllable length. Spherical nanoparticles of UO_2 could be obtained from the reduction of U(VI) precursor with different solvent ratio in autoclaves while proper Ce-doping could significantly alter the growth mode of these nanoparticles and obvious variation in the HER performance can be observed from the doping. These well-established synthetic methods provide a solid base for the further study and utilization of uranium in various applications.

Experimental Section

Materials: Uranium acetate ($UO_2(CH_3COO)_2 \cdot 2H_2O$) was purchased from Dingtian Chemical Co. of Shijiazhuang, Hebei Province, China; octadecene was purchased from Alfa Aesar Chemicals. Oleic acid, oleylamine, ethanol, cyclohexane, *n*-hexane, *n*-heptane, *n*-decane, chloroform, and toluene were all purchased from Sinopharm Chemical Reagent Co. Ltd.

Synthesis of Ultrathin Nanoribbons: In a typical reaction, uranium acetate (0.106 g) was dissolved in a mixture of oleylamine (OM, 5 mL) and oleic acid (OA, 1 mL) at 100 °C in a 25-mL flask with a pin-hole in the cap, yielding a clear yellowish solution. The solution was then heated to 150 °C under magnetic stirring and kept for 4 h before cooling down. Aliquots were sampled out at specific reaction time and quickly injected into 1-mL acetone. It was then centrifuged at 10 000 rpm for 10 min and the precipitate was redispersed in cyclohexane and precipitated by adding equal amount of ethanol and then went through two more rounds of centrifugation. The final product was dispersed in cyclohexane and stored for characterization. For the synthesis of wide ultrathin nanoribbons, the reaction mixture was similarly dissolved and the solution was first transferred into an 11-mL autoclave and sealed before heating in the oven for the same time. The final product was washed in a similar way of dissolution and centrifugation before redispersed in cyclohexane.

Synthesis of Ultrathin Nanowires: In a typical reaction, uranium acetate (0.530 g) was dissolved in OM (2 mL) at 100 °C and mixed with OA (1 mL) within a 25-mL flask, yielding a clear yellowish solution. The solution was then transferred into an 11-mL autoclave, mixed with 3 mL octadecene, and stirred for 3 min. The mixture was then sealed and heated in the oven at 180 °C for 2 h. After cooling down, the final product was centrifuged at 10 000 rpm for 10 min and the precipitate redispersed in cyclohexane and precipitated by adding equal amount of ethanol then went through two more rounds of centrifugation. The final product was dispersed in cyclohexane and stored for characterization.

Synthesis of Near-Spherical Nanoparticles: In a typical reaction, uranium acetate (0.265 g) was dissolved in OM (2 mL) at 100 °C and mixed with OA (4 mL) within a 25-mL flask, yielding a clear yellowish solution. The solution was then transferred into an 11-mL autoclave, mixed with 3 mL octadecene, and stirred for 3 min. The mixture was then sealed and heated in the oven at 180 °C for 4 h before cooling down. The product was then centrifuged at 10 000 rpm for 10 min after mixing with equal amount of ethanol; the precipitate was redispersed in cyclohexane and precipitated again by adding equal amount of ethanol and then went through two more rounds of centrifugation. The final product was dispersed in cyclohexane and stored for characterization.

Synthesis of Cerium-Doped Nanoparticles: The procedures were identical to that of near-spherical nanoparticles except that ammonium cerium (IV) nitrate ($Ce(NH_4)_2(NO_3)_6$) was codissolved with uranium acetate according to specified molar ratio.

Electrochemical Characterizations: Electrochemical studies were carried out in a standard three-electrode system controlled by a Princeton PARSTAT P4000 of AMETEK Co. Ltd. electrochemistry workstation. 5 mg of the catalyst was dispersed in 730 μL of water, 220 μL of ethanol, and 50 μL of 5 wt% Nafion solution by at least 30 min sonication to form a homogeneous ink. Then 5 μL of the catalyst ink (loading about 25 μg of the catalyst) was loaded onto a glassy carbon electrode with 5 mm in diameter and used as the working electrode, a graphite paper (1 × 5 cm) the counter electrode and saturated calomel electrode as the reference electrode. The reference was calibrated and converted to reversible hydrogen electrode. First, the catalyst was cycled more than 50 times by cyclic voltammetry (CV) until a stable CV curve was formed to ensure the stability of the electrode for the following test. Linear sweep voltammetry was carried out at 5 mV s^{-1} for the polarization curves. AC impedance measurements were carried out in the same configuration at $\eta = -0.45$ V (vs RHE) from 10^5 to 0.1 Hz. All of the measurements were under hydrogen flowing and the working electrode (RDE) continuously rotated at 1600 rpm to get rid of the hydrogen bubbles.

Supporting Information

Supporting Information is available from the Wiley Online Library or from the author.

Acknowledgements

[1] a) C. B. Murray, D. J. Norris, M. G. Bawendi, *J. Am. Chem. Soc.* **1993**, *115*, 8706; b) X. G. Peng, L. Manna, W. D. Yang, J. Wickham, E. Scher, A. Kadavanich, A. P. Alivisatos, *Nature (London)* **2000**, *404*, 59; c) S. H. Sun, C. B. Murray, D. Weller, L. Folks, A. Moser, *Science* **2000**, *287*, 1989; d) X. Wang, J. Zhuang, Q. Peng, Y. D. Li, *Nature (London)* **2005**, *437*, 121; e) S. E. Habas, H. Lee, V. Radmilovic, G. A. Somorjai, P. Yang, *Nat. Mater.* **2007**, *6*, 692; f) Z. Y. Huo, C. K. Tsung, W. Y. Huang, X. F. Zhang, P. D. Yang, *Nano Lett.* **2008**, *8*, 2041; g) L. Cademartiri, G. Guerin, K. J. M. Bishop, M. A. Winnik, G. A. Ozin, *J. Am. Chem. Soc.* **2012**, *134*, 9327; h) S. Hu, H. Liu, P. Wang, X. Wang, *J. Am. Chem. Soc.* **2013**, *135*, 11115.

[2] a) M. Law, L. E. Greene, J. C. Johnson, R. Saykally, P. D. Yang, *Nat. Mater.* **2005**, *4*, 455; b) M. Bruchez, M. Moronne, P. Gin, S. Weiss, A. P. Alivisatos, *Science* **1998**, *281*, 2013; c) R. Plass, S. Pelet, J. Krueger, M. Grätzel, U. Bach, *J. Phys. Chem. B* **2002**, *106*, 7578; d) X. Feng, L. Feng, M. Jin, J. Zhai, L. Jiang, D. Zhu, *J. Am. Chem. Soc.* **2003**, *126*, 62; e) T. A. Kandiel, A. Feldhoff, L. Robben, R. Dillert, D. W. Bahnemann, *Chem. Mater.* **2010**, *22*, 2050; f) C. Hagleitner, A. Hierlemann, D. Lange, A. Kummer, N. Kerness, O. Brand, H. Baltes, *Nature (London)* **2001**, *414*, 293.

[3] a) H. M. Wu, Y. G. Yang, Y. C. Cao, *J. Am. Chem. Soc.* **2006**, *128*, 16522; b) H. Wu, O. Chen, J. Zhuang, J. Lynch, D. LaMontagne, Y. Nagaoka, Y. C. Cao, *J. Am. Chem. Soc.* **2011**, *133*, 14327; c) T. M. Nenoff, B. W. Jacobs, D. B. Robinson, P. P. Provencio, J. Huang, S. Ferreira, D. J. Hanson, *Chem. Mater.* **2011**, *23*, 5185.

[4] T. T. Meek, B. Von Roedern, *Vacuum* **2008**, *83*, 226.

[5] a) H. Idriss, *Surf. Sci. Rep.* **2010**, *65*, 67; b) A. P. Amrute, F. Krumeich, C. Mondelli, J. Pérez-Ramírez, *Chem. Sci.* **2013**, *4*, 2209; c) G. J. Hutchings, C. S. Heneghan, I. D. Hudson, S. H. Taylor, *Nature (London)* **1996**, *384*, 341; d) A. R. Fox, S. C. Bart, K. Meyer, C. C. Cummins, *Nature (London)* **2008**, *455*, 341; e) F. Krumeich, A. P. Amrute, C. Mondelli, J. Pérez-Ramírez, *Z. Anorg. Allg. Chem.* **2014**, *640*, 768.

[6] a) A. P. Alivisatos, *Science* **1996**, *271*, 933; b) S. Hu, X. Wang, *Chem. Soc. Rev.* **2013**, *42*, 5577.

[7] C. Walther, M. A. Denecke, *Chem. Rev.* **2013**, *113*, 995.

[8] D. Hudry, J.-C. Griveau, C. Apostolidis, O. Walter, E. Colineau, G. Rasmussen, D. Wang, V. S. K. Chakravadhaluna, E. Courtois, C. Kübel, *Nano Res.* **2014**, *7*, 119.

[9] a) D. Su, M. Wieske, E. Beckmann, A. Blume, G. Mestl, R. Schlögl, *Catal. Lett.* **2001**, *75*, 81; b) D. Wang, D. S. Su, R. Schlögl, *Z. Anorg. Allg. Chem.* **2004**, *630*, 1007; c) S. Hu, X. Ling, T. Lan, X. Wang, *Chem. Eur. J.* **2010**, *16*, 1889.

[10] K. Grossmann, T. Arnold, R. Steudtner, S. Weiss, G. Bernhard, *Naturwissenschaften* **2009**, *96*, 963.

[11] R. T. Shannon, *Acta Crystallogr. A* **1976**, *32*, 751.

[12] a) Y. Dong, M. Kapilashrami, Y. Zhang, J. Guo, *CrystEngComm* **2013**, *15*, 10657; b) K. Jayanthi, S. Chawla, K. N. Sood, M. Chhibara, S. Singh, *Appl. Surf. Sci.* **2009**, *255*, 5869.